Viral Retinopathy in Experimental Models of Zika Infection

Zhenyang Zhao,[1] Matthew Yang,[1] Sasha R. Azar,[2] Lynn Soong,[3] Scott C. Weaver,[3–5] Jiaren Sun,[3] Yan Chen,[1] Shannan L. Rossi,[3–5] and Jiyang Cai[1]

[1]Department of Ophthalmology & Visual Sciences, University of Texas Medical Branch, Galveston, Texas, United States
[2]Institute for Translational Sciences, University of Texas Medical Branch, Galveston, Texas, United States
[3]Department of Microbiology & Immunology, University of Texas Medical Branch, Galveston, Texas, United States
[4]Department of Pathology, University of Texas Medical Branch, Galveston, Texas, United States
[5]Institute for Human Infections and Immunity, University of Texas Medical Branch, Galveston, Texas, United States

Correspondence: Shannan L. Rossi, Department of Pathology, University of Texas Medical Branch, 301 University Boulevard, Galveston, TX 77555-1075, USA; slrossi@utmb.edu.
Jiyang Cai, Department of Ophthalmology & Visual Sciences, University of Texas Medical Branch, 301 University Boulevard, Galveston, TX 77555-1102, USA; jicai@utmb.edu.

Submitted: April 10, 2017
Accepted: July 10, 2017

Citation: Zhao Z, Yang M, Azar SR, et al. Viral retinopathy in experimental models of zika infection. *Invest Ophthalmol Vis Sci*. 2017;58:4075–4085. DOI:10.1167/iovs.17-22016

Purpose. Emerging evidence has shown that both congenital and adult Zika virus (ZIKV) infection can cause eye diseases. The goals of the current study were to explore mechanisms and pathophysiology of ZIKV-induced eye defects.

Methods. Wild-type or A129 interferon type I receptor–deficient mice were infected by either FSS13025 or Mex1-7 strain of ZIKV. Retinal histopathology was measured at different time points after infection. The presence of viral RNA and protein in the retina was determined by in situ hybridization and immunofluorescence staining, respectively. Growth curves of ZIKV in permissive retinal cells were assessed in cultured retinal pigment epithelial (RPE) and Müller glial cells.

Results. ZIKV-infected mice developed a spectrum of ocular pathologies that affected multiple layers of the retina. A primary target of ZIKV in the eye was Müller glial cells, which displayed decreased neurotrophic function and increased expression of proinflammatory cytokines after infection. ZIKV also infected RPE; and both the RPE and Müller cells expressed viral entry receptors TYRO3 and AXL. Retinitis, focal retinal degeneration, and ganglion cell loss were observed after the clearance of viral particles.

Conclusions. Our data suggest that ZIKV can infect infant eyes with immature blood–retinal barrier and cause structural damages to the retina. The ocular findings in microcephalic infants may not be solely caused by ZIKV-induced impairment of neurodevelopment.

Keywords: Zika virus, Axl, Tyro 3, Müller cell, RPE

With formidable teratogenic effects, Zika virus (ZIKV) has gained global attention since the first American outbreak in Brazil.[1] Vertical transmission of ZIKV during pregnancy can cause a myriad of malformations exemplified by microcephaly. Ocular abnormalities, including microphthalmia, as well as chorioretinal atrophy and gross pigmentation, have been identified in 34% to 55% of infants with microcephaly.[2,3] Eye signs and symptoms in adult ZIKV infection have also been reported, with viral RNAs detected in both serum and aqueous humor of the patient.[4] ZIKV infection in the eye can affect any part of the uveal tract (iris, ciliary body, retina, and choroid), while most clinical cases have defects in the posterior segment.[5–7] There was a case report of severe vision decline after ZIKV infection.[4] Beyond the clinical findings, mechanisms of ZIKV pathogenesis in the eye are unclear. Long-term visual prognosis, as well as the social and economic impact, in affected infants remains largely unknown.[8,9]

ZIKV is a member of the genus *Flavivirus*, which includes the human pathogens dengue and West Nile viruses that are known to cause various ocular diseases in humans.[10–12] The type I interferon (IFN) response is a major defense mechanism against most flaviviruses. A129 mice, which are deficient in IFN receptors α and β (*Ifnar*$^{-/-}$), have been commonly used as a mouse model to study ZIKV infection.[13,14] A recent study by Miner et al.[15] reported that ZIKV-infected A129 mice developed eye inflammation with retinal enrichment of viral RNA. However, the ocular cell tropism of ZIKV was not fully elaborated and the study did not monitor long-term damage to retinal structure.[15]

In this current study, we examined eyes of A129 mice infected by two strains of ZIKV. Our results showed that infected animals developed retinal viral infiltration, posterior uveitis, and damages to the photoreceptor neurons and retinal ganglion cells (RGCs). ZIKV preferentially infected retinal pigment epithelial (RPE) and Müller cells, impaired their neurotrophic functions, and elicited retinal inflammatory responses. Eyes infected by the Mex1-7 strain of ZIKV developed long-term pathology such as focal loss of RGCs and optic nerve axonal neuropathy. Our work identified specific retinal cell targets and described the detailed pathologic process of ZIKV eye infection. This knowledge is critical for understanding the mechanisms of ZIKV-induced eye diseases and for developing effective treatments.

Methods

Animals

Animal protocols were approved by the Institutional Animal Care and Use Committee (IACUC) of the University of Texas

Medical Branch (UTMB). All procedures were conducted in accordance with the ARVO Statement for the Use of Animals in Ophthalmic and Vision Research. A129 mice were obtained from a colony at UTMB and were maintained under pathogen-free caging and reared until the desired age. Wild-type C57BL/6J mice were initially purchased from Jackson Lab (Bar Harbor, ME, USA). Mice were inoculated with 100 µL ZIKV diluted to 1×10^6 plaque-forming units (PFU)/mL in phosphate-buffered saline (PBS) via the intraperitoneal route.[13] Daily checks were performed on mice to monitor for signs of illness and morbidity. All mice meeting moribund criteria (tremors, paralysis, severe lethargy, and/or >20% weight loss) were euthanized.[13] At the time of necropsy, mice were euthanized by CO_2 asphyxiation and exsanguinated by intracardiac puncture. One eye was harvested for viral titration and the other was fixed in 4% paraformaldehyde for at least 24 hours prior to histology.

Viruses

The ZIKV Mex1-7 strain ($ZIKV^{MEX}$) was isolated from a pool of *Aedes* mosquitoes from Mexico in 2015[16] and passaged three times in Vero cells prior to use. The FSS13025 strain of ZIKV ($ZIKV^{FSS}$) was obtained from the World Reference Collection for Emerging Viruses and Arboviruses (WRCEVA) cultivated at UTMB. $ZIKV^{FSS}$ was passaged in the following cell lines prior to use: 1× AP-1, 1× C6/36, and 5× Vero 2.

Cell Culture

Primary cultures of mouse retinal Müller cells were established from neonatal mice (postnatal day [P]3–P5), following established methods with modifications.[17–20] Briefly, retina tissues were dislodged into single-cell suspension after collagenase (Worthington Biochemical, Lakewood, NJ, USA) digestion, filtered through 40-µm nylon strainer (Thermo Fisher Scientific, Waltham, MA, USA), and collected by centrifugation. Cells were cultured in Dulbecco's modified Eagle's medium (DMEM)/F12 containing 20% fetal bovine serum (FBS) (Sigma-Aldrich Corp., St. Louis, MO, USA), 20% L929 cell–conditioned medium, 2 mM Glutamax (Thermo Fisher Scientific), 100 U/mL penicillin and streptomycin. After 10 to 14 days in culture, cells were treated with 0.05% trypsin-EDTA for 1 minute at 37°C. Microglia remained attached to the plate.[18] The majority of dissociated cells were glutamine synthetase (GS)-positive Müller cells[21] and were used for the in vitro infection experiments without further passaging.

Primary cultures of human fetal RPE (hfRPE) cells were established as previously described.[22] Cells were grown and passaged in alpha-modified Eagle's medium (α-MEM) containing 10% FBS and N1 supplements (Sigma-Aldrich Corp.). Before seeding, the plates and wells were coated with collagen (STEMCELL Technologies, Vancouver, BC, Canada). Cells between passages 3 and 6 were used for experiments. Viral infection was performed in growth media at 10:1 multiplicity of infection (MOI) for 1 hour. Afterward the viral inoculation was removed and cells were replenished with fresh medium.

Titrations of Tissues and Serum Viral Load

Upon necropsy, one eye with the optic nerve was collected and homogenized with TissueLyser II (QIAGEN, Hilden, Germany). Blood from the sample animal was spun at 3000*g* for 5 minutes and serum was transferred to a separate tube. All titrations were performed as previously described.[13] Briefly, Vero cell monolayers were infected with 10-fold serial dilutions of samples for 1 hour, followed by overlaying of semisolid 4% methylcellulose in DMEM. Cultures were incubated for 3 days prior to removing the overlay, washed once with PBS, and fixed with a 50:50 vol/vol mixture of methanol and acetone for 30 minutes. ZIKV-infected foci were visualized by immunohistochemistry.[13] Final titers were reported as PFU/mL serum or PFU/g tissue. The average eye weight of 0.016 g was used for calculations.

Histology and Immunofluorescence Microscopy

Paraffin sections of posterior eyes were prepared as described previously.[23] Sagittal sections of 4-µm thickness were cut from cornea to optic nerve and stained with hematoxylin and eosin (H&E). For immunofluorescent labeling, an antigen retrieval step was performed by boiling sections in 10 mM sodium citrate buffer (pH 6.2) (Thermo Fisher Scientific) for 20 minutes. The sources of antibodies used for the study are listed in Supplementary Table S1. Fluorescence images were acquired on a Carl Zeiss Observer Z1 microscope (Thornwood, NY, USA) equipped with Apotome and ZEN imaging software.

Dual Fluorescent RNA In Situ Hybridization

In situ hybridization was performed with the ViewRNA ISH tissue assay kit (Affymetrix, Cleveland, OH, USA), following the manufacturer's recommendations. Sections of 8-µm thickness were deparaffinized and digested with protease at 40°C for 15 minutes to unmask the RNA targets. Two sets of RNA probes, targeting either ZIKV polyprotein (VF1-19981-06) or GS (VB6-16850-06), were hybridized with the samples for 2 hours at 40°C. Alkaline phosphatase–conjugated detection probes and signal amplifiers were used in sequential reactions to develop signals from gene-specific probes. ZIKV polyprotein was visualized after chromogenic reaction with fast red substrate, which showed red color in bright-field and fluoresced in Cy3 channel. GS staining was visualized as blue in bright-field and fluorescent in the far red channel.

Magnetic Activated Cell Sorting (MACS)

Müller cells were isolated using the MACS cell separation system (Miltenyi Biotec, San Diego, CA, USA). $ZIKV^{FSS}$-infected retina tissues were harvested at 6 days post infection (dpi) and digested with collagenase. The cell suspension was first labeled with FITC-conjugated anti-CD44 antibody (eBioscience, San Diego, CA, USA), followed by binding to magnetic bead-conjugated anti-FITC antibody. Tagged cells were isolated with a MidiMACS column (Miltenyi Biotec, San Diego, CA, USA). Both Müller cells and flow-through fractions were collected for downstream RT-PCR analyses.

RNA Isolation, cDNA Synthesis, and Quantitative RT-PCR

Total RNA was isolated with TRIzol reagent (Thermo Fisher Scientific) and treated with DNase (Ambion, Austin, TX, USA) to remove residual trace of genomic DNA. Complementary DNA (cDNA) was synthesized from 0.2 to 1 µg total RNA using random hexamer (Promega, Madison, WI, USA). Gene-specific primers used for RT-PCR amplification are listed in Supplementary Table S2. Quantitative RT-PCR was performed on an ABS 7500 real-time PCR system (Applied Biosystems, Foster City, CA, USA). Results were presented as fold change after normalization to the expression level of *β-actin*.[22]

Small Interfering RNA (siRNA)

SiRNA duplexes were designed and synthesized by Integrated DNA Technologies (Coralville, IA, USA). Sequences of siRNA

are listed in Supplementary Table S3. Cells were transfected with 100 pmol siRNA duplexes by Lipofectamine 2000 (Thermo Fisher Scientific). Forty-eight hours after transfection, cells were used for ZIKV infection at MOI of 10:1. Viral RNA expression was measured by quantitative RT-PCR 24 hours thereafter.

Western Blot Analyses

Cells were lysed in buffer containing CelLyticM cell lysis reagent (Sigma-Aldrich Corp.) and 2× Laemmli sample buffer (Bio-Rad, Hercules, CA, USA) at 1:1 ratio, 10 mM glycerophosphate, 10 mM pyrophosphate, 1 mM NaF, 1 mM Na_3VO_4, and protease inhibitor cocktails. After sonication, samples were resolved on SDS-PAGE and transferred to nitrocellulose membranes (Bio-Rad). Membranes were probed with antibodies against ZIKV envelope protein (ENV) (BioFront Technologies, Tallahassee, FL, USA), AXL, TYRO3 (Cell Signaling Technology, Danvers, MA, USA), and β-actin (Sigma-Aldrich Corp.). Signals were detected by an Odyssey Infrared Imaging System (LI-COR, Lincoln, NE, USA).[22]

Statistical Analyses

All experiments were repeated at least three times. Data were analyzed with the GraphPad Software (La Jolla, CA, USA) and presented as mean ± SEM. The significance of differences between two groups was evaluated using a Student's *t*-test. For multiple comparisons, 1-way ANOVA followed by Tukey's multiple comparison tests was used. Differences were considered statistically significant when the *P* value was less than 0.05.

Results

ZIKV Retinopathy in Young A129 Mice

We employed two strains of ZIKV to study the mechanism of viral pathogenesis in the eye. $ZIKV^{FSS}$ is a member of the Asian lineage and shares >98% nucleotide sequence identity with all American strains.[24] $ZIKV^{MEX}$ was isolated from a pool of *Aedes aegypti* mosquitoes from the first outbreak in Mexico in 2015.[16] When A129 mice were infected by $ZIKV^{FSS}$ at the time of weaning (3 weeks), viral ENV was detected at 4 dpi around the blood–ocular barrier sites in the ciliary body, major retinal vessels, and underneath the RPE (Fig. 1A). At 6 dpi, $ZIKV^{FSS}$ broke through the barrier and spread to focal areas of the retina, and ENV was detected in the nerve fiber layer, inner nuclei, inner plexiform, and the RPE (Figs. 1B, 2G, Supplementary Fig. S1B). Infectious viral particles were found in the eyes of $ZIKV^{FSS}$-infected mice on day 4 but waned to nearly undetectable levels by day 6 (Fig. 1C). Most infected animals in this group were euthanized after 6 dpi due to excessive weight loss and/or neurologic signs of illness such as tremors, paralysis, or severe lethargy.[13]

Compared to $ZIKV^{FSS}$, the contemporary $ZIKV^{MEX}$ strain caused relatively moderate systemic signs and lower viremia. However, high levels of infectious particles ($\sim 3.6 \times 10^6$ PFU) persisted in the eye tissue 1 week after the clearance of viremia, suggesting prolonged replication within an immunologically privileged site (Fig. 1C). At 9 dpi, retinal viral antigen staining of $ZIKV^{MEX}$ was comparable to that in 6-dpi $ZIKV^{FSS}$-infected eyes (Figs. 1D, Supplementary Fig. S1D). Viral infiltration progressed dramatically with time, and $ZIKV^{MEX}$ infected the entire thickness of the neural retina by 17 dpi (Fig. 1D, Supplementary Fig. S1E). Only young A129 mice were susceptible to ZIKV. When infection was performed in 11-week-old A129 mice, no viral staining was found in the retina (Supplementary Fig. S1C).

We next infected newborn wild-type mice 5 to 14 days after birth, and measured the presence of ZIKV ENV in the retina at 6 and 9 dpi. Viral ENV staining was detected in the retina only at 6 dpi (Fig. 1E). The infectivity rapidly decreased with postnatal age. Retinas from 5-day-old mice showed diffuse staining patterns of viral ENV protein, but only small numbers of cells were infected in the retina of 7-day-old mice (Fig. 1E). Thus, ZIKV infection of the retina was confirmed in both A129 and immunocompetent mice. However, given the constraints of developing a model based upon 5-day-old mice, we chose to continue the mechanism and pathology studies with young A129 mice.

Müller Cells and RPE as ZIKV Host Cells in the Retina

After confirming the presence of ZIKV in the retinal tissue, we next examined the viral tropism in major retinal cells. The branching staining pattern of ZIKV in the inner retina first prompted us to focus on the astrocytes and Müller cells (Fig. 2A). On immunostaining of retinal sections, both $ZIKV^{FSS}$ and $ZIKV^{MEX}$ ENV showed colocalization with glial fibrillary acidic protein (GFAP), a marker protein of astrocytes and activated Müller cells (Figs. 2B, 2C). This was further validated with costaining of GS, a Müller cell–specific marker (Fig. 2D).[21] Müller gliosis was preceded by the appearance of $ZIKV^{MEX}$ ENV protein (Fig. 2C). ENV staining was also detected in the RPE (Fig. 2G), consistent with the previously reported focal RPE change in both congenital and acquired cases of human eye infection.[7,25] Ionized calcium binding adapter molecule 1 (Iba1)-positive retinal microglia/macrophages increased with time, but did not show costaining of viral protein (Fig. 2E). Occasional ganglion cell infection was identified, but the photoreceptor neurons were not infected (Fig. 2F).

The presence of viral RNA in the infected cells was measured by in situ hybridization, using probe specific for ZIKV RNA.[15] Müller cells were labeled in the same reaction with a probe specific for *GS* gene. Consistent with the data from immunostaining, ZIKV RNA was detected in Müller cells that expressed mRNA for *GS* in A129 mice infected with the $ZIKV^{MEX}$ (Fig. 3A). Next we measured viral RNA expression in retinal Müller cells purified from $ZIKV^{FSS}$-infected mice, with MACS and anti-CD44 antibody.[26,27] The enrichment of Müller cells was validated by their expression of *GS* RNA. Consistent with the data of immunostaining and in situ hybridization, purified Müller cells showed robust RNA expression of both nonstructural (NS) proteins *NS1*, *NS4*, and viral polymerase (Fig. 3B). Thus, with three independent approaches we have shown that ZIKV infected retinal Müller cells.

In addition to the in vivo experiments, we used cultured RPE and Müller cells for in vitro ZIKV infection. Infected RPE and Müller cells expressed ENV and NS1 proteins, as shown by immunostaining (Figs. 4A, 4B, Supplementary Figs. S2A, S2B) and Western blot analyses (Fig. 4C). The presence of replication-competent ZIKV in culture supernatant fractions of infected cells was further determined by a standard focus forming assay in Vero cells.[13] As shown in Figure 4D, viral titers had a time-dependent increase in supernates from RPE cells infected with either $ZIKV^{FSS}$ or $ZIKV^{MEX}$, indicating that RPE cells were highly permissive to productive infection. Of note, there was no significant time-dependent increase of viral titer in the supernates of ZIKV-inoculated Müller cells.

Previous studies reported that entry of ZIKV into cells was dependent on cell surface receptors including CD209/DC-SIGN, TIM1, TYRO3, and AXL.[28] Both RPE and Müller cells

Investigative Ophthalmology & Visual Science

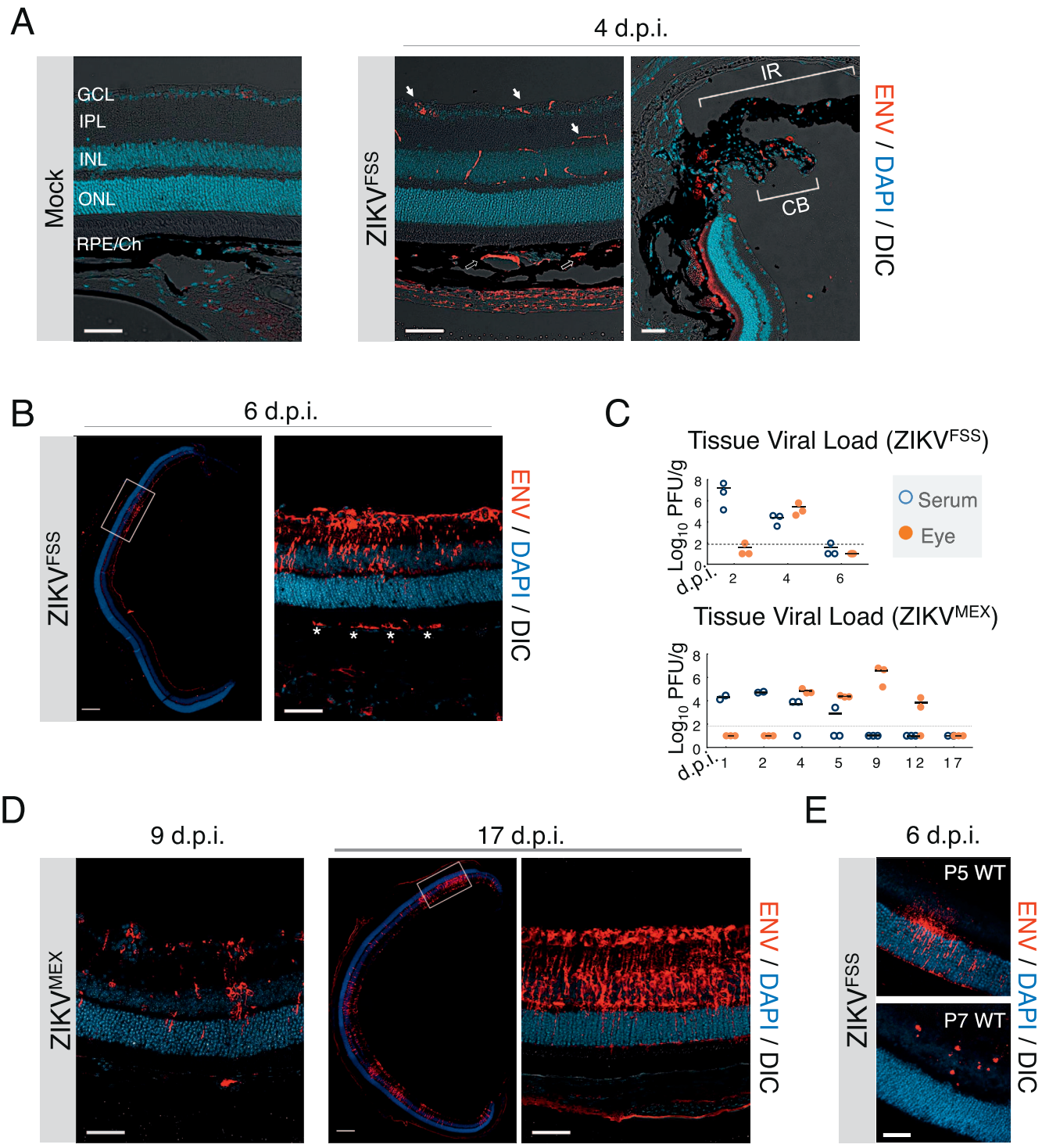

Figure 1. ZIKV infection of A129 and wild-type mice at weaning. (**A**, **B**, **D**) Immunostaining of viral ENV at indicated times after inoculation by either the ZIKV^{FSS} or ZIKV^{MEX} in A129 mice. *Arrows*, retinal vessels; *open arrows*, choroidal vessels; *asterisks*, RPE infection. IR, iris; CB, ciliary body; GCL, ganglion cell layer; IPL, inner plexiform layer; INL, inner nuclear layer; ONL, outer nuclear layer; CH, choroid. (**C**) Viral titer from eye and serum of the same animal. Each data point on plot C represents one infected animal. (**E**) ENV staining of retina from wild-type mice of indicated postnatal (P) age infected with ZIKV^{FSS}. *Scale bars*: lower magnification, 200 µm (**B**, **D**); 50 µm (**A**, **C**, **E**).

expressed TYRO3 and AXL (Figs. 4C, 4E). While TIM1 is considered as an entry coreceptor for ZIKV,[29] we did not detect TIM1 transcripts in examined tissues (Fig. 4E), indicating low, if any, expression in the posterior eye. There was weak expression of CD209, a C-type lectin receptor, in RPE tissues (Fig. 4E). Cultured retinal microglia, however, did not express the TAM family receptors (Fig. 4E), which is consistent with their lack of ZIKV infection in vivo (Fig. 2E). Knockdown of both *TYRO3* and *AXL* by siRNA suppressed the amount of viral RNA in cultured Müller or RPE cells infected by ZIKV (Fig. 4F). The average efficiency of gene knockdown by siRNA was approximately 40%. Altogether, these data support-

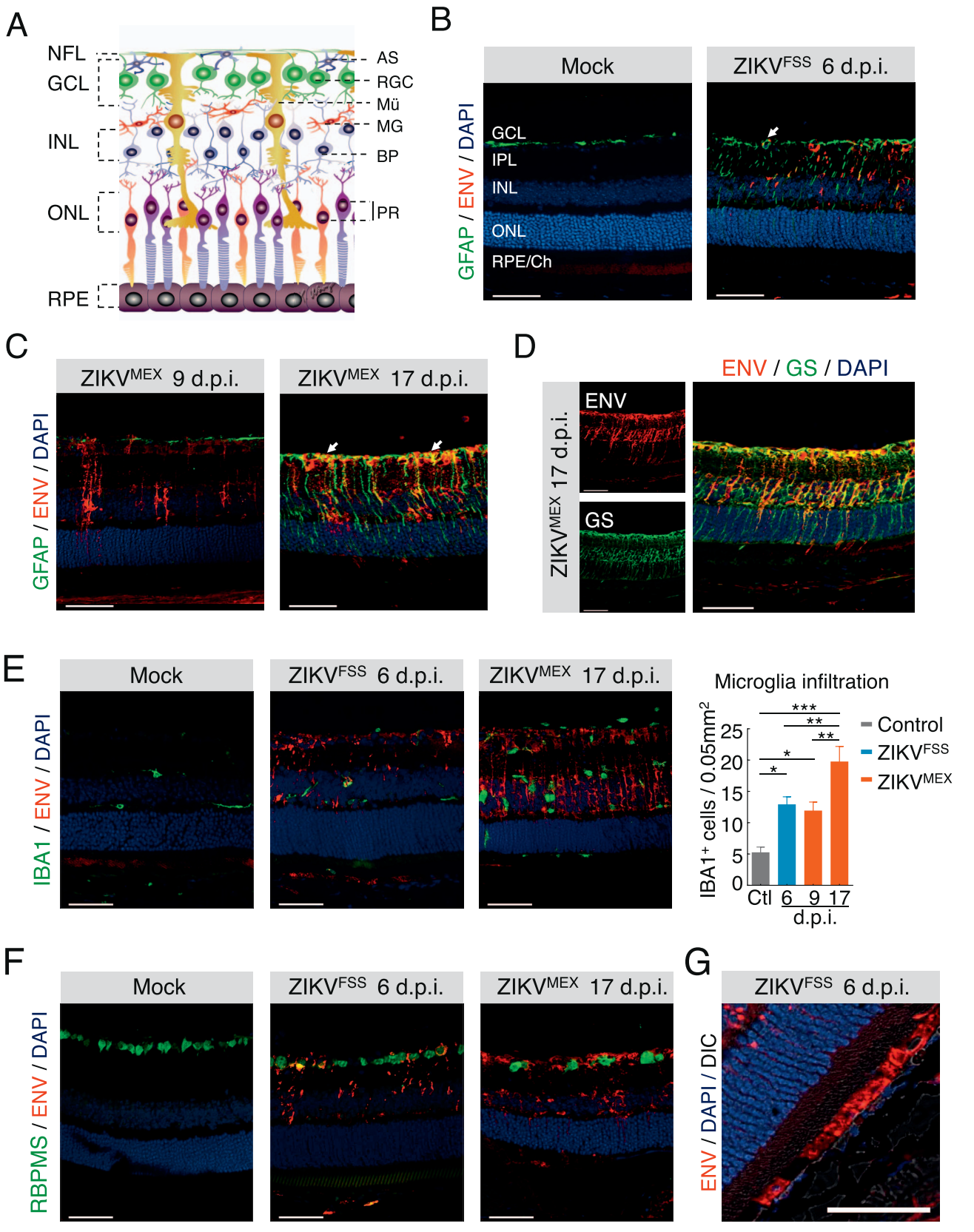

Figure 2. Cell type specificity of ZIKV infection in the retina. (**A**) Retinal structure outlined by a schematic illustration. AS, astrocyte; RGC, retinal ganglion cell; Mü, Müller cell; MG, microglia; BP, bipolar cell; PR, photoreceptors. (**B**–**F**) Dual immunostaining of ZIKV ENV with cell type–specific markers, including GFAP for astrocytes and activated Müller cells (**B**, **C**), GS for total Müller cells (**D**), IBA1 for microglia (**E**), and RBPMS for ganglion cells (**F**). (**G**) ENV staining in the RPE. Quantification of infiltrated microglia was performed at different time points after infection. Each time point represents at least three infected animals. $^{*}P < 0.05$; $^{**}P < 0.01$. 1-way ANOVA and Bonferroni post hoc test. *Scale bars*: 50 µm.

Investigative Ophthalmology & Visual Science

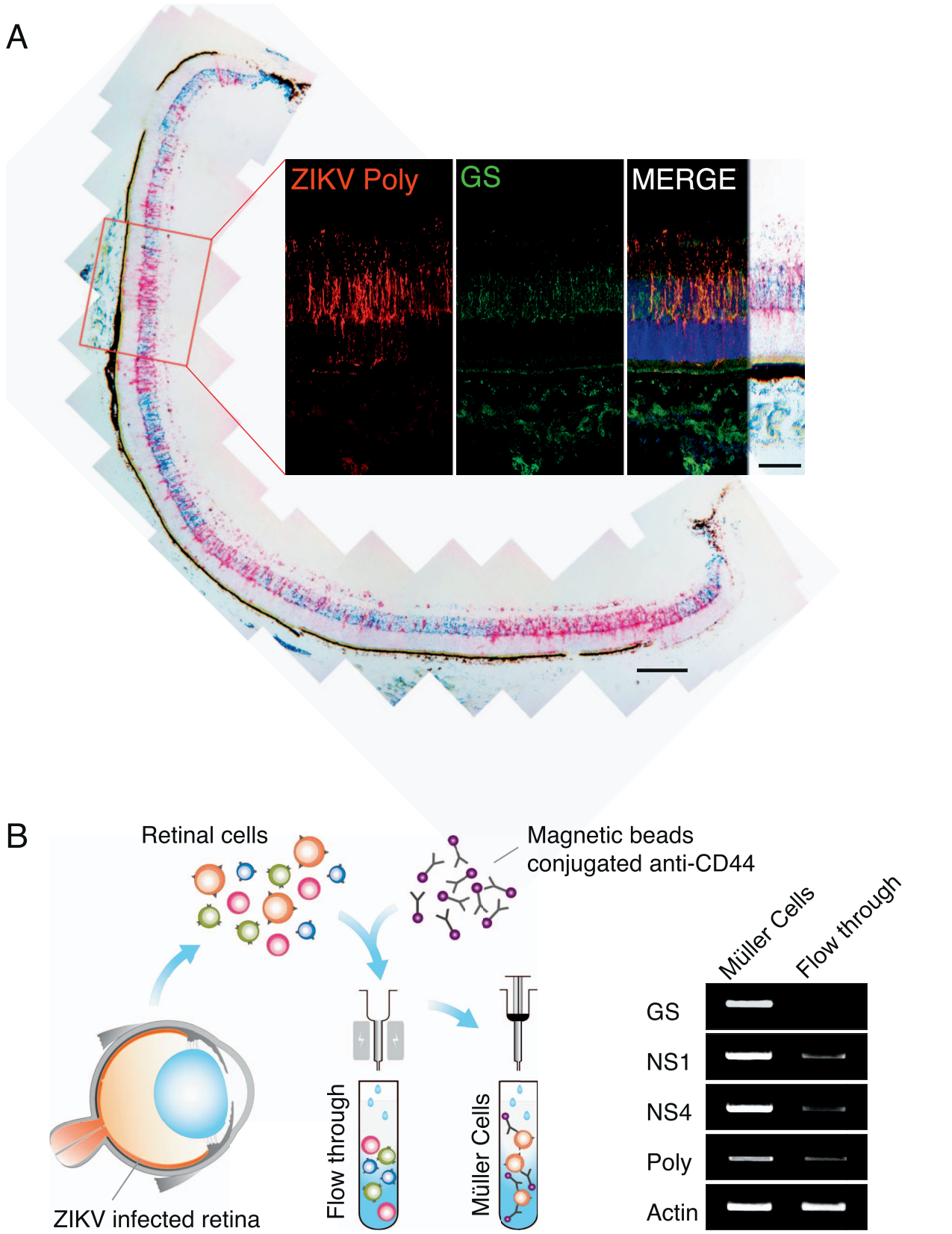

Figure 3. ZIKV RNA in retinal Müller cells. (**A**) Dual staining of ZIKV polyprotein (*red*) and GS (*blue*) RNA by in situ hybridization, in retina of a 3-week-old A129 mice infected by $ZIKV^{MEX}$ at 17 dpi. Fluorescent images of the *boxed area* were enlarged to illustrate the colocalization. (**B**) Schematic illustration of magnetic activated cell sorting of Müller cells from ZIKV-infected retina. RT-PCR analyses of ZIKV RNA and Müller cell marker in both isolated Müller cells and flow-through fraction. RNA was isolated from A129 mice infected by $ZIKV^{FSS}$ at 6 dpi. *Scale bars*: 200 μm (**A**); *inset* = 50 μm.

Investigative Ophthalmology & Visual Science

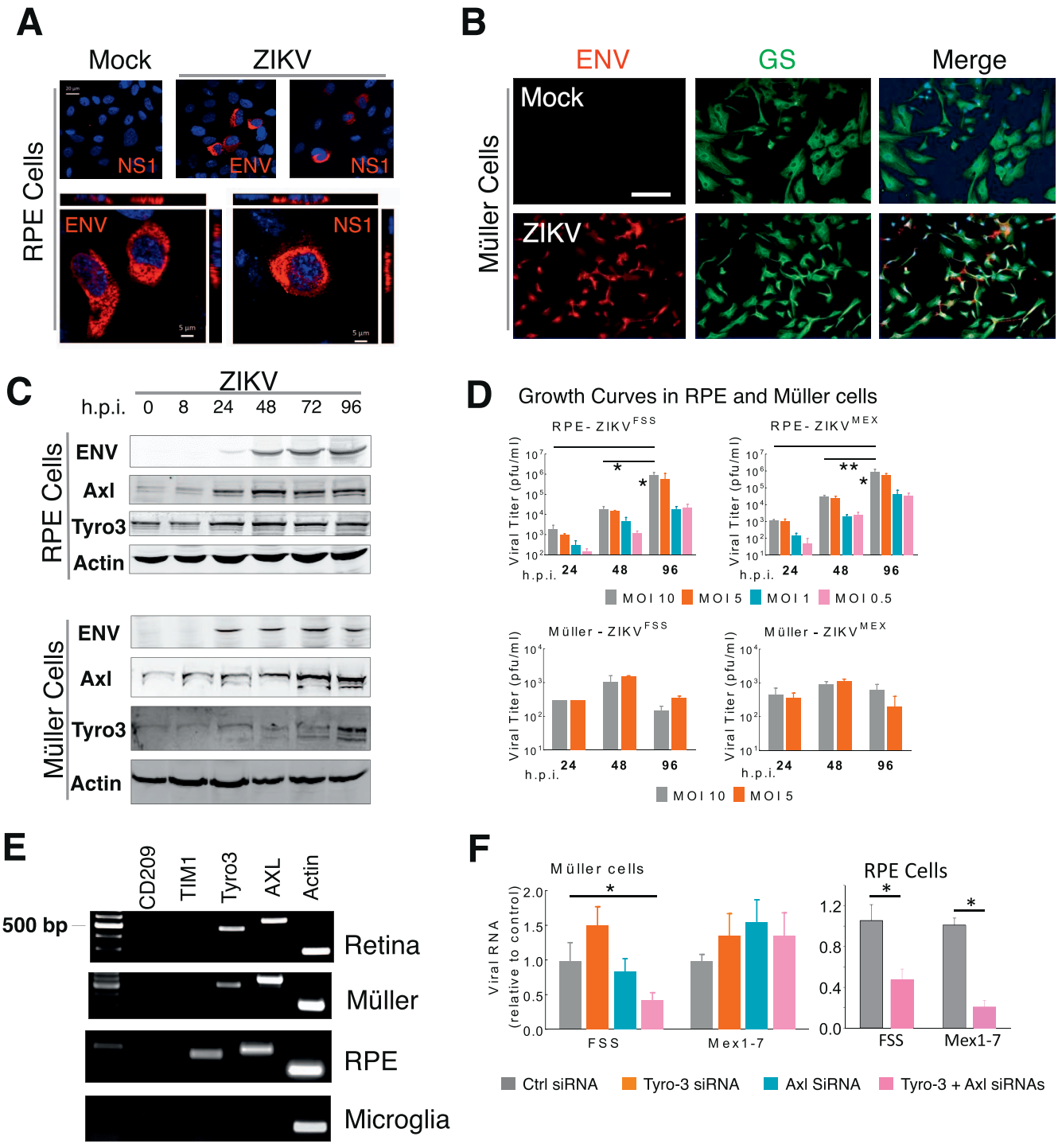

Figure 4. ZIKV infection of cultured retinal cells. (**A**) Immunostaining of viral ENV or NS1 in cultured human fetal RPE cells at 2 dpi by ZIKV^{FSS}. *Bottom*: reconstitutions of series of Z-stack images at higher magnification. *Blue*: nuclei. (**B**) Immunostaining of primary retinal Müller cells infected with ZIKV^{FSS}. (**C**) Western blot analyses of expression of viral proteins, AXL and TYRO3 receptors in infected cells. (**D**) Growth curves of ZIKV^{FSS} or ZIKV^{MEX} in RPE and Müller cells. (**E**) RT-PCR analyses of mRNA expression of potential viral entry receptors in retinal and RPE tissues from 1-month-old A129 mice (*top*), or cultured primary mice retinal Müller and microglial cells (*bottom*). (**F**) Quantitative RT-PCR analyses of viral RNA in Müller cells transfected with siRNA targeting TYRO3 and/or AXL. Data presented are the average from three separate experiments. *Scale bars*: 20 μm (**A**, *upper*), 5 μm (**A**, *lower*); 50 μm (**B**).

ed RPE and Müller as major target cells for ZIKV infection. RPE is highly permissive to ZIKV and could be a major source of active viral production at early time points. Müller cells can be chronically infected but probably do not support productive infection.

ZIKV-Induced Müller Cell Dysfunction and Neuronal Loss

Müller glia have essential neural supporting functions, such as secretion of neurotrophic factors and removal of excessive

Investigative Ophthalmology & Visual Science

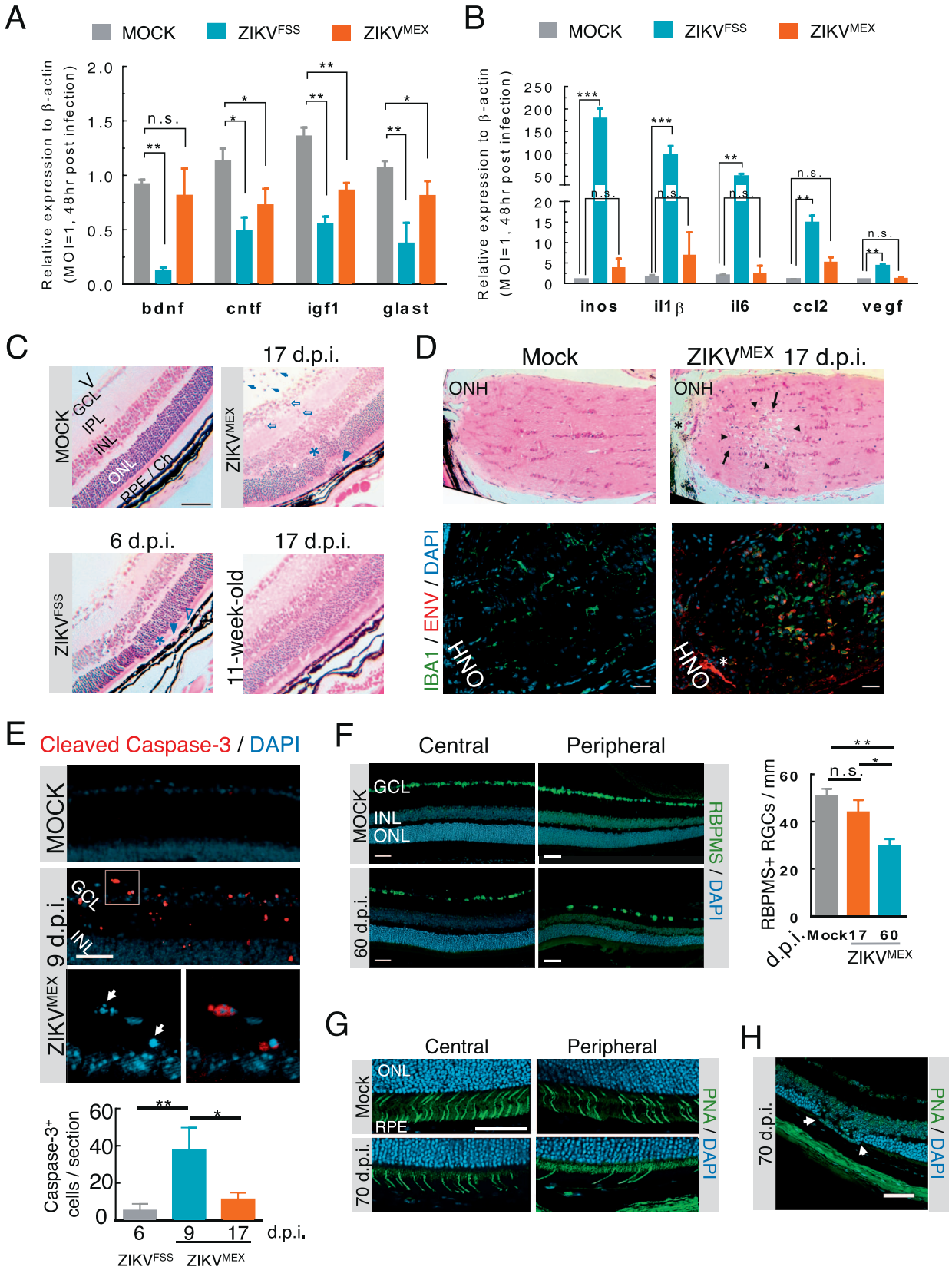

Figure 5. Functional consequences of ZIKV infection of the retina. (**A**, **B**) Quantitative RT-PCR analyses of neurotrophic and proinflammatory gene expression in cultured Müller cells infected with either ZIKV^{FSS} or ZIKV^{MEX} ($n = 4$). (**C**) H&E-stained retinal histology sections from infected A129 mice. The age of the animals was either 3 or 11 weeks at time of viral inoculation. V, vitreous cavity. *Arrows*: intravitreal infiltrates; *open arrows*: retinitis with cell infiltration; *asterisks*: outer nuclear layer damage; *arrowheads*: subretinal inflammatory cells; *open arrowheads*: RPE defects. (**D**) H&E-stained sections of the optic nerve head (ONH). Immediately neighboring sections were stained for viral ENV and IBA1^{+} cell infiltration. *Arrowheads*: necrotic lesion; *arrows*: mononuclear cell infiltrate; *asterisk*: same blood vessel on adjacent sections. (**E**) Representative micrograph

of cleaved caspase-3 staining. The *boxed area* at the *top* was enlarged to show nuclear condensation and fragmentation (*arrows*). Caspase-3-positive cells were quantified on six slides from each animal ($n = 4$ each group). (**F**) Immunostaining of central and peripheral retinal ganglion cells from mock- or $ZIKV^{MEX}$-infected mice at 60 dpi. Quantitative data were based on the average number of RBPMS-positive cells on 10 retinal sections ($n = 3$ each group). (**G**) Staining of cone cells by peanut agglutinin (PNA) at central and peripheral retina. (**H**) Focal photoreceptor degeneration. *Scale bars*: 100 μm (**C**, **D**); 50 μm (**E**–**H**). Data were analyzed by 1-way ANOVA with Turkey post hoc test. $^{*}P < 0.05$, $^{**}P < 0.001$.

glutamate to prevent excitotoxicity.[30,31] Active Müller gliosis is an early sign of retinal stress and insults.[30] To explore the functional consequences of ZIKV infection, we measured the expression of neurotrophic factors, glutamate transporter, and inflammatory markers in cultured Müller cells. $ZIKV^{FSS}$ decreased the expression of brain-derived neurotrophic factor (*BDNF*), ciliary neurotrophic factor (*CNTF*), insulin-like growth factor 1 (*IGF1*), and glutamate transporter L-glutamate/L-aspartate transporter (*GLAST*) (Fig. 5A). Similar changes occurred in $ZIKV^{MEX}$-infected Müller cells, although to a lesser extent. Expression of proinflammatory genes and cytokines, including *iNOS*, *IL6*, and *CCL2*, was upregulated by $ZIKV^{FSS}$ but not $ZIKV^{MEX}$ (Fig. 5B, Supplementary Fig. S2C).

Histopathologic examinations showed that eyes of A129 mice infected by $ZIKV^{FSS}$ mainly displayed signs of posterior uveitis, including intravitreal and retinal infiltrates and focal RPE defects (Fig. 5C, Supplementary Fig. S3). A129 mice at 11 weeks of age were resistant to ocular $ZIKV^{FSS}$ infection as their eyes showed no sign of abnormality (Fig. 5C). $ZIKV^{MEX}$ induced more severe ocular pathologic changes with heavy infiltrates, retinitis, photoreceptor loss, and RPE defects at both 9 and 17 dpi of $ZIKV^{MEX}$ (Fig. 5C, Supplementary Figs. S2B, S2C). Optic nerve viral infiltration and axonal neuropathy were observed in 17-dpi samples with extensive $IBA1^{+}$ infiltrating cells on the immediate adjacent section (Fig. 5D). Caspase-3 activation was detected in the nerve fiber layer and inner nuclear layer peaking at 9 dpi, indicating apoptosis of astrocytes or infiltrated macrophages in the vitreous (Fig. 5E).

The long-term sequelae of compromised neural support by Müller cells and RPE, and the proinflammatory microenvironment in the retina, resulted in significant loss of cone photoreceptors and ganglion cells after ZIKV infection, most prominent in the peripheral sites in 60- and 70-dpi samples (Figs. 5F, 5G, Supplementary Fig. S4). Focal degeneration of the outer nuclear layer was likely caused by RPE infection (Fig. 5H). Aside from significant RGC loss, most retinal inflammation regressed at 60 dpi (75% ZIKV-infected mice) with residual intravitreal cells and positive viral staining only around ciliary bodies (Supplementary Fig. S4). In one animal, delayed viral clearance was associated with severe retinal damage at 70 dpi (Supplementary Fig. S4C). The findings suggest that permanent retinal structural damage can occur after neonatal ZIKV infection.

Discussion

In recent years, numerous clinical studies have reported retinal infection and posterior uveitis caused by emerging and re-emerging viruses,[32] such as Ebola,[33,34] West Nile,[35,36] Chikungunya,[37] dengue,[12] and ZIKV.[5,6] Viral persistence in the ocular tissue is a potential threat of disease transmission,[15,33] and can lead to long-term irreversible damages to the neural retina. ZIKV infection is congenital. However, a recent study showed that in mice with intrauterine infection, viral RNA was detectable in brain 1 week after birth, and the well-developed retina of these animals still showed progressive degeneration during the first 2 months after birth.[38] A recent clinical study also reported that some of the ZIKV-infected infants showed microcephaly around 1 year after birth.[39] Therefore, it is likely that, in addition to the developmental defects, neuroinflammation and degeneration in adult retina and brain will contribute to ZIKV-induced pathology and functional defects.

Data from our current study show that, before the blood–retinal barrier and host immunity are well developed,[40] ZIKV may enter the retinal tissue and establish an infection of susceptible cell populations (Figs. 1–3) and eventually lead to irreversible retinal injury (Fig. 5). ZIKV preferentially infects RPE and Müller cells (Figs. 2, 4), which are key supporting cells for neuronal survival, function, and injury repair in the retina.[30] Müller cell ablation causes neuronal and vascular pathologic effects resembling ocular features of congenital ZIKV eye disease.[41] Viral RNA was detected in Müller cells by in situ hybridization and RT-PCR (Fig. 3), suggesting that the presence of ZIKV ENV was not due to engulfing neighboring infected cell debris.

Organs with immune privilege, such as brain, testis, placenta, and the posterior eye, tend to have higher viral loads and are more prone to ZIKV-induced tissue damage in A129 mice.[13] Initial viral entry appeared through both the RPE (Fig. 2G) and the pigmented ciliary epithelium (Fig. 1A); viral spread may involve the breakdown of the blood–retinal barrier or blood–aqueous barrier at either site. The eyes of 11-week-old A129 mice were not infected by ZIKV (Supplementary Fig. S1C), suggesting that the ocular barrier exerted protection in adult mice. On the other hand, the IFN responses in mice are much more robust than those in primates, due to the differences in viral protease-mediated cleavage of STING, a viral RNA sensor that initiates the IFN responses.[42] Future studies will be needed to further define whether similar mechanisms of ZIKV pathogenesis are applicable to humans or nonhuman primates.

Previously ZIKV had not been considered as a major health threat, and infection in adults usually caused moderate clinical symptoms and signs, like Zika fever and skin rash, which are self-resolved. In the current ZIKV outbreak in the Americas, however, infected newborns have developed severe neurologic complications, in particular microcephaly, and a wide spectrum of ocular abnormalities.[2,3] The route of vertical transmission and the time of infection that occurred during early stages of gestation and fetal development were determining factors of the clinical outcomes. On the other hand, it is also possible that ZIKV gained pathogenicity through mutations in its genome as it spread to the Americas. The latter is supported by our findings that the more contemporary $ZIKV^{MEX}$ strain displayed distinct properties in infected mice.

While viremia and tissue viral load of $ZIKV^{FSS}$ were transient, $ZIKV^{MEX}$ proteins and RNA were detected in the retina long after viremia had subsided (Fig. 1C). The persistent infection caused Müller gliosis (Figs. 2B, 2C) and structural damage to the RGCs and optic nerve axons (Fig. 5). In contrast, retinal pathology was not observed in $ZIKV^{FSS}$-infected eyes (Fig. 5C) and was not reported in the recently published study by Miner and colleagues.[15] Strain differences were also reported by a recent study that compared differential gene expression in cultured neural progenitor cells infected by either $ZIKV^{FSS}$ or an African strain MR766.[43] The underlying molecular mechanisms of strain-specific differences in pathologic effects, as well as the functional consequences of viral infection in specialized neuronal tissues, will be further

Investigative Ophthalmology & Visual Science

explored in future studies. It is also possible that ZIKV^{MEX} is a unique isolate among strains in the Americas. If so, genetic differences in the virus will provide insightful details as to the progression of long-term ocular ZIKV sequelae.

In summary, our studies have shown that ZIKV can infect the retina in both immunodeficient and immunocompetent mice. Infection with the ZIKV^{MEX} strain caused structural damage to the neuronal tissues in the retina that likely has long-term effects on visual function. Müller and RPE cells are the main host cells of ZIKV in the retina. A better understanding of the mechanisms of viral pathogenesis in susceptible retinal cells, and further characterization of the strain differences, will benefit the development of novel target-based therapy against ZIKV.

Acknowledgments

Supported by National Institutes of Health Grants EY 026999 (YC), EY 021937 (JC), and AI 120942 (SCW); the International Retina Research Foundation; and Carl Marshall & Mildred Almen Reeves Foundation.

Disclosure: **Z. Zhao**, None; **M. Yang**, None; **S.R. Azar**, None; **L. Soong**, None; **S.C. Weaver**, None; **J. Sun**, None; **Y. Chen**, None; **S.L. Rossi**, None; **J. Cai**, None

References

1. Schuler-Faccini L, Ribeiro EM, Feitosa IM, et al. Possible association between Zika virus infection and microcephaly – Brazil, 2015. *MMWR Morb Mortal Wkly Rep*. 2016;65:59–62.
2. de Paula Freitas B, de Oliveira Dias JR, Prazeres J, et al. Ocular findings in infants with microcephaly associated with presumed Zika virus congenital infection in Salvador, Brazil. *JAMA Ophthalmol*. 2016;134:529–535.
3. Ventura CV, Maia M, Travassos SB, et al. Risk factors associated with the ophthalmoscopic findings identified in infants with presumed Zika virus congenital infection. *JAMA Ophthalmol*. 2016;134:912–918.
4. Furtado JM, Esposito DL, Klein TM, Teixeira-Pinto T, da Fonseca BA. Uveitis associated with Zika virus infection. *N Engl J Med*. 2016;375:394–396.
5. Ventura CV, Maia M, Bravo-Filho V, Gois AL, Belfort R Jr. Zika virus in Brazil and macular atrophy in a child with microcephaly. *Lancet*. 2016;387:228.
6. Miranda HA II, Costa MC, Frazao MA, Simao N, Franchischini S, Moshfeghi DM. Expanded spectrum of congenital ocular findings in microcephaly with presumed Zika infection. *Ophthalmology*. 2016;123:1788–1794.
7. Ventura CV, Maia M, Ventura BV, et al. Ophthalmological findings in infants with microcephaly and presumable intra-uterus Zika virus infection. *Arq Bras Oftalmol*. 2016;79:1–3.
8. Besnard M, Eyrolle-Guignot D, Guillemette-Artur P, et al. Congenital cerebral malformations and dysfunction in fetuses and newborns following the 2013 to 2014 Zika virus epidemic in French Polynesia. *Euro Surveill*. 2016;21:13.30181.
9. Moshfeghi DM, de Miranda HA II, Costa MC. Zika virus, microcephaly, and ocular findings. *JAMA Ophthalmol*. 2016;134:945.
10. Khairallah M, Chee SP, Rathinam SR, Attia S, Nadella V. Novel infectious agents causing uveitis. *Int Ophthalmol*. 2010;30:465–483.
11. Sivakumar RR, Prajna L, Arya LK, et al. Molecular diagnosis and ocular imaging of West Nile virus retinitis and neuroretinitis. *Ophthalmology*. 2013;120:1820–1826.
12. Yip VC, Sanjay S, Koh YT. Ophthalmic complications of dengue Fever: a systematic review. *Ophthalmol Ther*. 2012;1:2.
13. Rossi SL, Tesh RB, Azar SR, et al. Characterization of a novel murine model to study Zika virus. *Am J Trop Med Hyg*. 2016;94:1362–1369.
14. Dowall SD, Graham VA, Rayner E, et al. A susceptible mouse model for Zika virus infection. *PLoS Negl Trop Dis*. 2016;10:e0004658.
15. Miner JJ, Sene A, Richner JM, et al. Zika virus infection in mice causes panuveitis with shedding of virus in tears. *Cell Rep*. 2016;16:3208–3218.
16. Guerbois M, Fernandez-Salas I, Azar SR, et al. Outbreak of Zika virus infection, Chiapas State, Mexico, 2015, and first confirmed transmission by Aedes aegypti mosquitoes in the Americas. *J Infect Dis*. 2016;214:1349–1356.
17. Li L, Qu C, Wang F. A novel method for co-culture with Muller cells and microglia in rat retina in vitro. *Biomed Rep*. 2015;3:25–27.
18. Saura J, Tusell JM, Serratosa J. High-yield isolation of murine microglia by mild trypsinization. *Glia*. 2003;44:183–189.
19. Jiang T, Chang Q, Zhao Z, et al. Melatonin-mediated cytoprotection against hyperglycemic injury in Muller cells. *PLoS One*. 2012;7:e50661.
20. Yanni SE, McCollum GW, Penn JS. Genetic deletion of COX-2 diminishes VEGF production in mouse retinal Muller cells. *Exp Eye Res*. 2010;91:34–41.
21. Riepe RE, Norenburg MD. Muller cell localisation of glutamine synthetase in rat retina. *Nature*. 1977;268:654–655.
22. Yu B, Xu P, Zhao Z, Cai J, Sternberg P, Chen Y. Subcellular distribution and activity of mechanistic target of rapamycin in aged retinal pigment epithelium. *Invest Ophthalmol Vis Sci*. 2014;55:8638–8650.
23. Zhao Z, Xu P, Jie Z, et al. γδ T cells as a major source of IL-17 production during age-dependent RPE degeneration. *Invest Ophthalmol Vis Sci*. 2014;55:6580–6589.
24. Cunha MS, Esposito DL, Rocco IM, et al. First complete genome sequence of Zika virus (Flaviviridae, Flavivirus) from an autochthonous transmission in Brazil. *Genome Announc*. 2016;4:e00032-16.
25. Kodati S, Palmore TN, Spellman FA, Cunningham D, Weistrop B, Sen HN. Bilateral posterior uveitis associated with Zika virus infection. *Lancet*. 2017;389:125–126.
26. Shinoe T, Kuribayashi H, Saya H, Seiki M, Aburatani H, Watanabe S. Identification of CD44 as a cell surface marker for Muller glia precursor cells. *J Neurochem*. 2010;115:1633–1642.
27. Greenberg KP, Geller SF, Schaffer DV, Flannery JG. Targeted transgene expression in muller glia of normal and diseased retinas using lentiviral vectors. *Invest Ophthalmol Vis Sci*. 2007;48:1844–1852.
28. Hamel R, Dejarnac O, Wichit S, et al. Biology of Zika virus infection in human skin cells. *J Virol*. 2015;89:8880–8896.
29. Tabata T, Petitt M, Puerta-Guardo H, et al. Zika virus targets different primary human placental cells, suggesting two routes for vertical transmission. *Cell Host Microbe*. 2016.
30. Bringmann A, Pannicke T, Grosche J, et al. Muller cells in the healthy and diseased retina. *Prog Retin Eye Res*. 2006;25:397–424.
31. Bringmann A, Iandiev I, Pannicke T, et al. Cellular signaling and factors involved in Muller cell gliosis: neuroprotective and detrimental effects. *Prog Retin Eye Res*. 2009;28:423–451.
32. de Andrade GC, Ventura CV, Mello Filho PA, Maia M, Vianello S, Rodrigues EB. Arboviruses and the eye. *Int J Retina Vitreous*. 2017;3:4.
33. Varkey JB, Shantha JG, Crozier I, et al. Persistence of Ebola virus in ocular fluid during convalescence. *N Engl J Med*. 2015;372:2423–2427.

34. Steptoe PJ, Scott JT, Baxter JM, et al. Novel retinal lesion in Ebola survivors, Sierra Leone, 2016. *Emerg Infect Dis*. 2017; 23:1102–1109.
35. Chan CK, Limstrom SA, Tarasewicz DG, Lin SG. Ocular features of west nile virus infection in North America: a study of 14 eyes. *Ophthalmology*. 2006;113:1539–1546.
36. Hasbun R, Garcia MN, Kellaway J, et al. West Nile virus retinopathy and associations with long term neurological and neurocognitive sequelae. *PLoS One*. 2016;11:e0148898.
37. Mahendradas P, Ranganna SK, Shetty R, et al. Ocular manifestations associated with chikungunya. *Ophthalmology*. 2008;115:287–291.
38. Cui L, Zou P, Chen E, et al. Visual and motor deficits in grown-up mice with congenital Zika virus infection. *EBioMedicine*. 2017;20:193–201.
39. van der Linden V, Pessoa A, Dobyns W, et al. Description of 13 infants born during October 2015-January 2016 with congenital Zika virus infection without microcephaly at birth - Brazil. *MMWR Morb Mortal Wkly Rep*. 2016;65:1343–1348.
40. Yao H, Wang T, Deng J, Liu D, Li X, Deng J. The development of blood-retinal barrier during the interaction of astrocytes with vascular wall cells. *Neural Regen Res*. 2014;9:1047–1054.
41. Shen W, Fruttiger M, Zhu L, et al. Conditional Muller cell ablation causes independent neuronal and vascular pathologies in a novel transgenic model. *J Neurosci*. 2012;32:15715–15727.
42. Aguirre S, Maestre AM, Pagni S, et al. DENV inhibits type I IFN production in infected cells by cleaving human STING. *PLoS Pathog*. 2012;8:e1002934.
43. Zhang F, Hammack C, Ogden SC, et al. Molecular signatures associated with ZIKV exposure in human cortical neural progenitors. *Nucleic Acids Res*. 2016;44:8610–8620.

Investigative Ophthalmology & Visual Science